

A deep and wide-field view at the IC 2944 / 2948 complex in Centaurus [★]

G. Baume^{1,2}, M. J. Rodríguez², M. A. Corti^{1,3}, G. Carraro⁴, and J. A. Panei^{1,2} †

¹Facultad de Ciencias Astronómicas y Geofísicas - Universidad Nacional de La Plata, Paseo del Bosque S/N, La Plata, (B1900FWA), Argentina

²Instituto de Astrofísica de La Plata (CONICET-UNLP), Paseo del Bosque S/N, La Plata, (B1900FWA), Argentina

³Instituto Argentino de Radioastronomía (CONICET), Cno. Gral. Belgrano Km 40 (Parque Pereyra Iraola), Berazategui, Argentina

⁴ESO, Alonso de Córdova 3107, Vitacura, Santiago de Chile, Chile

Accepted 1988 December 15. Received 1988 December 14; in original form 1988 October 11

ABSTRACT

We employed the ESO MPI wide-field camera and obtained deep images in the VI_C passbands in the region of the IC 2944/2948 complex ($l \sim 294^\circ 8$; $b \sim -1^\circ 6$), and complemented them with literature and archival data. We used this material to derive the photometric, spectroscopic and kinematic properties of the brightest ($V < 16$) stars in the region. The VI deep photometry on the other end, helped us to unravel the lower main sequence of a few, possibly physical, star groups in the area.

Our analysis confirmed previous suggestions that the extinction toward this line of sight follows the normal law ($R_V = 3.1$). We could recognize B-type stars spread in distance from a few hundred pc to at least 2 kpc. We found two young groups (age ~ 3 Myr) located respectively at about 2.3 and 3.2 kpc from the Sun. They are characterized by a significant variable extinction (E_{B-V} ranging from 0.28 to 0.45 mag), and host a significant pre-main sequence population. We computed the initial mass functions for these groups and obtained slopes Γ from -0.94 to -1.02 ($e_\Gamma = 0.3$), in a scale where the classical Salpeter law is -1.35. We estimated the total mass of both main stellar groups in ~ 1100 and $\sim 500 M_\odot$, respectively. Our kinematic analysis indicated that both groups of stars deviate from the standard rotation curve of the Milky Way, in line with literature results for this specific Galactic direction.

Finally, along the same line of sight we identified a third group of early-type stars located at ~ 8 kpc from the Sun. This group might be located in the far side of the Sagittarius-Carina spiral arm.

Key words: (Galaxy:) open clusters and associations: general – (Galaxy:) open clusters and associations: individual: IC 2944 – IC 2948 Galaxy: structure – Stars: early-type – Stars: pre-main sequence – Stars: formation

1 INTRODUCTION

The study of young galactic clusters and HII regions is an essential tool to improve our understanding of key astrophysical processes like star formation, its modes, spatial variation, and duration (Lada & Lada 2003). At the same time, young star aggregates help us to probe the Galactic spiral structure, being one of the most prominent spiral arm tracers, together with gas, in the form of HI, HII, or CO (Carraro 2013).

Our group has focused its attention in recent years to several directions in the fourth quadrant of the Milky Way

–see e.g. Shorlin 1 (Carraro & Costa 2009), Danks 1 and 2 (Baume et al. 2009), NGC 6193/6167 (Baume et al. 2011) or CenOB1/NGC 4755 (Corti & Orellana 2013). In this paper we extend our study to the remarkable IC 2944/2948 region, located at $l \sim 294^\circ 8$ and $b \sim -1^\circ 6$.

IC 2944 is a nebula associated to the cluster Collinder 249 (Cr 249, C1134-627, or “ λ Cen cluster”) and it is centered on the star HD 101205. However, the designation IC 2944 is routinely used to identify the stellar group itself (see, e.g., *SIMBAD*¹, *WEBDA*²). The entire complex hosts the HII nebula IC 2948 and the stellar cluster Cr 249. The bright star λ Cen is also located in our covered field (see Fig. 1). According to Alter et al. (1970), the entire group of brightest stars in this region is also referred as Cen OB2 association.

[★] Based on observations collected at ESO La Silla, under program 076.D-0396

† E-mail: gbaume@fcaglp.unlp.edu.ar (GB), jimeno@fcaglp.unlp.edu.ar (MJR), mariela@fcaglp.unlp.edu.ar (MAC), gcarraro@eso.org (GC), panei@fcaglp.unlp.edu.ar (JAP)

¹ <http://simbad.u-strasbg.fr/simbad/>

² <http://www.univie.ac.at/webda/>

IC 2944/2948 appears then as a concentration of O stars (several of them identified as binary systems) and early B stars. Apparently, some of them are responsible for exciting the nebula. This area also contains Bok globules, that indicates the presence of an extremely young stellar population (Reipurth 2008).

The fundamental parameters of the various stellar groups have been matter of lively discussion in the literature, which prevented a general consensus on the star formation mode active in the region. Thackeray & Wesselink (1965) presented photoelectric photometry in the Johnson *UBV* system and determined radial velocities for 24 stars. They found a binary fraction greater than 50%. By using these 24 objects (19 stars located within 6' of the HD 101205 star and 5 O-type stars located outside this circle), they computed the following parameters: $\overline{E_{B-V}} = 0.33 \pm 0.06$, $V_0 - M_V = 11.5 \pm 0.2$ (~ 2 kpc) and a mean visual absorption of $0^m.50/\text{kpc}$ in this Galactic direction. On the other hand, Perry & Landolt (1986) studied several stars in this region using information in *V*, *uvby* and H_β bands, and claimed the stars to be a mere sample of early type field stars spread along the line of sight.

There is also poor agreement on the detailed structure of the complex, and the nature of the various apparent groups:

- Ardeberg & Maurice (1980, 1981) proposed that OB stars belong to various stellar groups at different distances along the line of sight. Specifically, they identify three groups: a) the closest at about 700 pc, b) seven bright stars that seem connected with HII region RWC62 at 1.7 kpc, and c) four more distant stars at 3-4 kpc.
- Walborn (1987) suggests that the O-type stars in the field of the HII region IC 2944 constitute a physical cluster. This group of O stars is the cause of the ionisation of the surrounding region.
- Later, McSwain & Gies (2005) argue for the existence of a cluster, based on *b*, *y* and H_α photometry. They estimated a distance of 1.8 kpc, an age of 6.6 Myr, and a reddening of $E_{B-V} \sim 0.32$.
- Reipurth et al. (1997) studied the globules discovered by Thackeray using CO observations and they revealed that the two larger globules are kinematically separated, and have masses of 4 and 11 M_\odot . However, they did not find evidences of active star formation. Accordingly, IC 2944 and IC 2948 would represent different parts of the same, large group of clouds surrounding a cluster of OB stars (Reipurth 2008).
- More recently, Nazé et al. (2013) studied for the first time this region using XMM-Newton data and claimed for the existence of a tight cluster.

In this paper we perform a detailed wide-field study of the region based on *UBVIJHK* data with other complementary spectroscopic and kinematic information. We use this material to derive updated estimates of the fundamental parameters of the various stellar groups. We also analyze this field in connection with other fields located on the fourth Galactic quadrant to derive information on the spiral structure in this portion of the disk.

The layout of the paper is as follows. In Sect. 2 we describe the data, and the reduction/calibration procedures. In Sect. 3 we present our analysis of the data together with several discussions. Finally, in Sect. 4 we summarize our conclusions.

2 DATA

This study makes use of the following material:

- Images, in VI_C bands, obtained with the Wide Field Imager

(WFI³) mounted at the Cassegrain focus of the MPG/ESO 2.2m Telescope at La Silla Observatory (Chile).

- Photometric data from the following surveys: APASS⁴ (Henden et al. 2010), 2MASS⁵ (Skrutskie et al. 2006) and XHIP (Anderson & Francis 2012).
- Spectroscopic classification for the brightest stars from the *SIMBAD* and *WEBDA* databases, and complemented with information from Kharchenko & Roeser (2009), Sana et al. (2011) and Sota et al. (2013).

2.1 Images

The WFI camera is a 4×2 mosaic of $2K \times 4K$ CCD detectors. The scale is $0'.238/\text{pix}$, and it covers a field of view (FOV) of $34'.0 \times 33'.0$ but, due to the narrow inter-chips gaps, the filling factor of each image is $\sim 95.9\%$. Images were acquired in 2006 during the nights of March 8th, April 25th and May 28th and the typical full width half maximum (FWHM) was in the range $0'.7 - 1'.4$, whereas air-masses values were 1.2 - 1.5. Details of the observations are given in Table 1.

All frames were pre-processed in the standard way using the IRAF⁶ task *ESOWFI/MSCREED*. That is, instrumental effects were corrected with calibration images (bias and sky-flats taken during the same observing runs).

2.2 Astrometry

World Coordinate System (WCS) header information of each frame was obtained using IRAF *MSCZERO* and *MSCCMATCH* tasks and UCAC4 data (Zacharias et al. 2013). This allowed us to obtain a reliable astrometric calibration. In order to go deep with our photometry, all the long exposures for each band were combined using IRAF *MSCIMAGE* task. This procedure helps to both removing cosmic rays and improving the signal-to-noise ratio for the faintest stars.

2.3 Photometry

Instrumental magnitudes were extracted using IRAF *DAOPHOT* and *PHOTCAL* packages, and employing the point spread function (PSF) method (Stetson 1987). Since the FOV is large, a quadratic spatially variable PSF was adopted and its calibration on each image was done using several isolated, spatially well distributed, bright stars (~ 20) across the field. The PSF photometry was finally aperture-corrected for each filter and exposure time. Aperture corrections were computed performing aperture photometry of the same stars used as PSF models. Finally, all resulting tables from different filters and exposures were combined using *DAOMASTER* (Stetson 1992) taking as reference the first night of observation (March 8th 2006).

Data for stars in common with our observations (about 300) were selected from the APASS catalog and their Sloan *gri* bands, and transformed to the VI_C system using the equations provided by Jester et al. (2005). Then, we used the following transformation equations to obtain the corresponding VI_C magnitudes from our

³ <http://www.eso.org/sci/facilities/lasilla/instruments/wfi.html>

⁴ <http://www.aavso.org/apass>

⁵ <http://irsa.ipac.caltech.edu/Missions/2mass.html>

⁶ IRAF is distributed by NOAO, which is operated by AURA under cooperative agreement with the NSF.

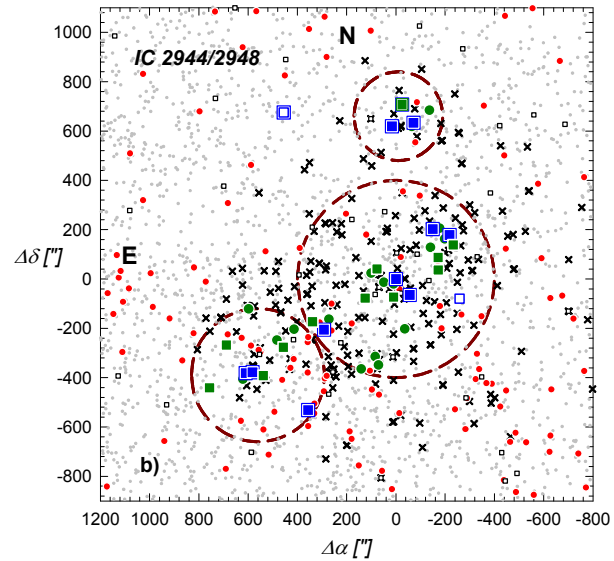
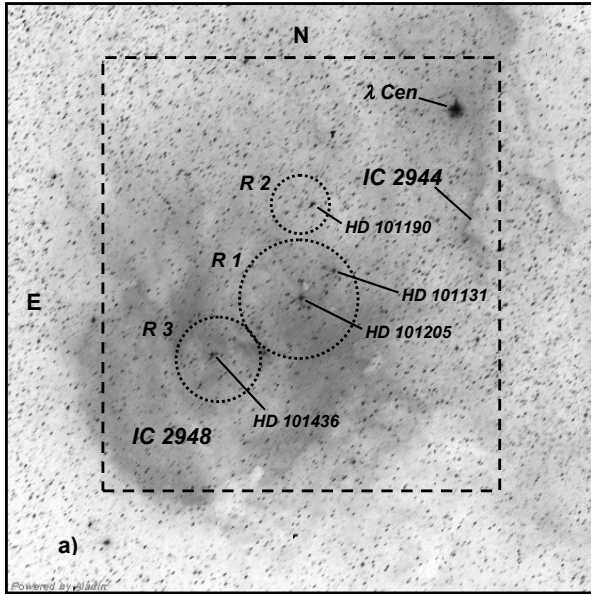


Figure 1. a) An *ALADIN* processed image from the Digitized Sky Survey (DSS). It is centered at HD 101205 ($\alpha_{J2000} = 11 : 38 : 20.4$; $\delta_{J2000} = -63 : 22 : 22.0$) and covering a field of $66'0 \times 66'0$. IC 2944/2948 HII regions and main O-type stars are identified. Big dashed square indicates the full studied area covered by our V_{IC} data ($44'6 \times 48'7$) whereas the dotted circles indicate the adopted *selected regions* (see text). b) Schematic central part of left panel showing stars ($V < 21$) as symbols. Squares and circles represent stars with and without known spectral classification respectively. Fill symbols indicate stars adopted as main two groups members (see text); blue and green symbols are O and B stars respectively. Double symbols indicate binary stars. X symbols and red dots are, respectively, x-ray sources (Nazé et al. 2013) and MSX sources (Lumsden et al. 2002) correlated with our data.

Table 1. Journal of observations of the scientific frames together with used calibration coefficients

Date	Frames	Exposure times [sec]×N	
		V	I_C
08/03/2006	short	-	10x9
	long	675x5	675x5
25/04/2006	short	10x9	-
	long	675x5	-
28/05/2006	short	-	-
	long	-	675x10
Calibration coefficients (08/03/2006)			
$v_1 = +1.044 \pm 0.006$	$i_1 = +1.951 \pm 0.009$		
$v_2 = +0.070 \pm 0.006$	$i_2 = -0.007 \pm 0.010$		

instrumental (v_i) ones:

$$v = V + v_1 + v_2(V - I_C) \quad (r.m.s. = 0.05)$$

$$i = I_C + i_1 + i_2(V - I_C) \quad (r.m.s. = 0.07)$$

with calibration coefficients presented in Table 1.

In order to obtain a reliable initial mass function (IMF, Sect. 3.7), we estimated the completeness of our optical data. The procedure was already used in our previous works (see e.g. Baume et al. 2003). Basically, we created several artificial images

by adding stars in random positions onto the original images using *ADDSTAR* routine of *DAOPHOT*. The added stars were distributed in luminosity as the real sample. In order to avoid overcrowding, in each experiment we added the equivalent to only about 15% of the original amount of stars. Since V band images are shallower than those in the I band, we have adopted for the latter the completeness factor (CF) estimated for V . The CF is defined then as the ratio between the number of artificial stars recovered and the number of artificial stars added, and our results are listed in Table 2,

2.4 Kinematic data

Radial velocity information for stars in the zone were extracted from different bibliographic sources and databases. In detail, we obtained heliocentric radial velocities for 50 stars: 3 stars from *SIMBAD* database, 19 from Kharchenko et al. (2007) and Kharchenko & Roeser (2009), 20 from Huang & Gies (2006), 4 from Thackeray & Wesselink (1965), 1 from Conti et al. (1977), 1 from Gies et al. (2002) and 2 stars from Sana et al. (2011). Regarding proper motions, all data were extracted from the UCAC4 catalog.

2.5 Mid-IR and X ray data

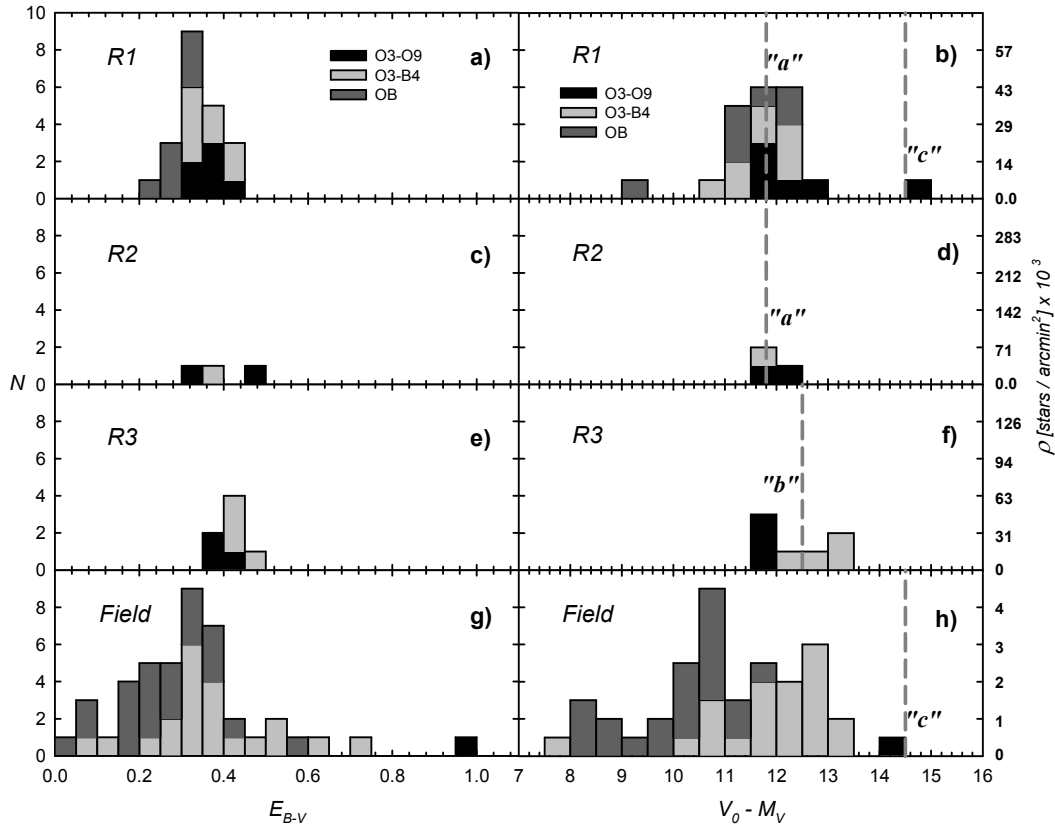
We cross-correlated our photometric data with mid-IR and X-ray data with the purpose of detecting pre-main sequence (PMS) stars (see also Sect 3.2.2).

As for the mid-R data, we use The Midcourse Space Experiment (MSX) data (Egan et al. 2003). MSX mapped the galactic plane and other regions missed or identified as particularly interest by the Infrared Astronomical Satellite (IRAS) at wavelengths of $4.29\mu m$, $4.35\mu m$, $8.28\mu m$, $12.13\mu m$, $14.65\mu m$, and $21.3\mu m$.

The Nazé et al. (2013) catalog was used for the X-ray data.

Table 2. Completeness Factors (CFs) of optical data

V	14-15	15-16	16-17	17-18	18-19	19-20	20-21	21-22	22-23	23-24
CF[%]	100	100	100	100	98	95	92	81	76	23

**Figure 2.** Distributions of the E_{B-V} and spectrophotometric $V_0 - M_V$ of OB stars with known ST and located inside the selected regions (see Fig. 1). Dashed lines in right panels indicate adopted $V_0 - M_V$ values for stellar groups/populations placed in each region. For a better understanding, the highest bar of panel a) means: two O3-O9 stars, six O3-B4 stars and nine OB stars.

These data were obtained using the X-ray Multi-Mirror Mission Newton (XMM-Newton) information. This data resulted by binning its three energy bands: *soft* = $S = 0.3 - 1.0$ keV, *medium* = $M = 1.0 - 2.0$ keV, and *hard* = $H = 2.0 - 10.0$ keV.

These data were cross-correlated with our optical data using *ALADIN*⁷ tool. To this aim, we use a $3''.0$ search radius for the XMM data, and a $10''.0$ radius for the MSX data –see Lumsden et al. (2002) and Nazé et al. (2013). We used the *all matches* option in *ALADIN* since this option gave us all the counterparts within the searching radius. Following these criteria, we found 139 counterparts in X-ray and 73 in mid-IR.

2.6 Final catalog

We used the *STILTS*⁸ tool to manipulate tables and we cross-correlated our V_{IC} data with the other public *UBVIJHK* photom-

etry and the available spectral classification. In this process, we adopted ESO/WFI V_{IC} data only for objects with $V > 13$. We obtained then a catalog with astrometric/photometric information of about 130,000 objects covering approximately a FOV of $44'.6 \times 48'.7$ around IC 2944/2948 (see Fig. 1). A more reliable analysis of the behavior of the Stellar Energy Distributions (SEDs) could be carried out with such a catalog (at least for brightest stars), thus preventing possible degeneracies in the photometric diagrams. The full catalog is presented in Table 3 which is available in electronic form at Centre de Données astronomiques de Strasbourg (CDS) web site.

3 ANALYSIS AND DISCUSSION

3.1 Selected regions

We started our study by identifying three regions where a visual over-density of early-type stars could be detected. These regions are shown as dotted circles in Fig. 1 and they are defined as follows:

⁷ <http://aladin.u-strasbg.fr/>

⁸ <http://www.star.bris.ac.uk/~mbt/stilts/>

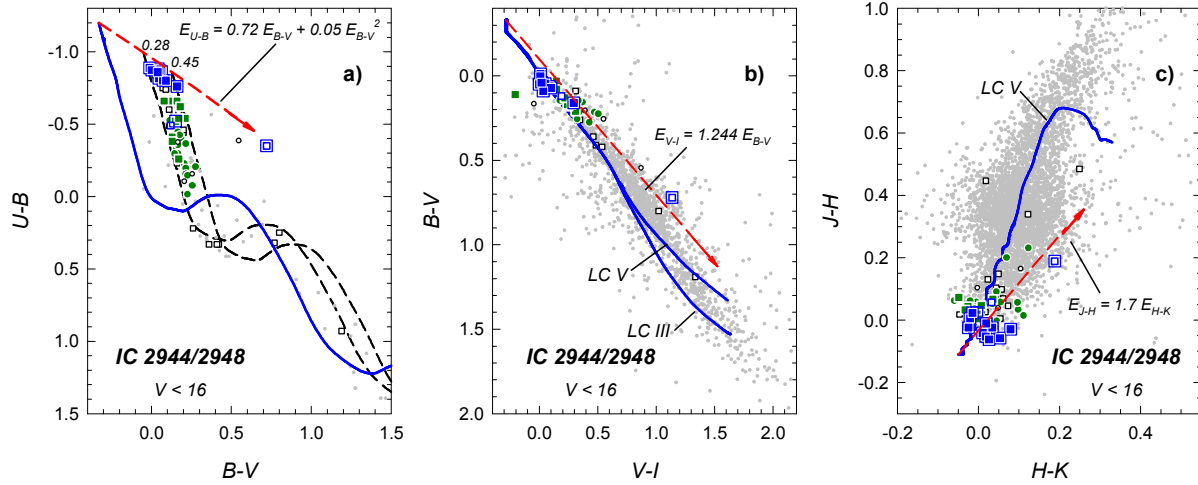


Figure 3. TCDs for the brightest stars ($V < 16$) in our sample. Symbols are as in Fig. 1b. The solid (blue) curve in plot a) is the Schmidt-Kaler (1982) ZAMS, while dashed (black) curves are the same ZAMS, but shifted along the reddening line (red) by the color excesses indicated above them. Solid (blue) curves in plot b) are intrinsic colors for luminosity class V and III from Cousins (1978a,b). Solid (blue) curve in plot c) are intrinsic colors for luminosity class V from Koornneef (1983). Dashed (red) arrows indicate the normal reddening path ($R_V = 3.1$).

- *Region 1 (R1)*: A circle centered at $\Delta\alpha = 0'0, \Delta\delta = 0'0$ and radius $400'0$
- *Region 2 (R2)*: A circle centered at $\Delta\alpha = -10'0, \Delta\delta = +660'0$ and radius $180'0$
- *Region 3 (R3)*: A circle centered at $\Delta\alpha = 560'0, \Delta\delta = -390'0$ and radius $270'0$

where we have used a coordinate system centered on HD 101205 star ($\Delta\alpha = (\alpha - \alpha_{HD101205}) \cos(\delta_{HD101205}); \Delta\delta = \delta - \delta_{HD101205}$).

3.2 Spectrophotometric study

3.2.1 Upper main sequence

Our compilation of spectroscopic data allowed us to estimate the distance and color excess of 162 stars located in our FOV. We applied then the traditional method (e.g. Corti et al. 2012) based on the absolute magnitude M_V and intrinsic colors calibration provided by Martins & Plez (2006) for O-type stars and by Schmidt-Kaler (1982) for B and later ones. We adopted an M_V uncertainty of 0.5 magnitude (Walborn 1972) and a value $R_V = A_V/E_{B-V} = 3.1$ (see in advance Fig. 3b). A linear interpolation was performed in case of missing calibration spectral type. In order to reduce the uncertainty, for binary systems, where both stars were classified (SB2), we obtained distance and color excesses by computing first the individual component magnitudes/colors and then we applied the above method. For binary systems with only one classification (SB1) we assumed our results have an additional minor uncertainty.

Computed distances and color excesses for known OB stars led us to the distributions presented in Fig. 2, where we noticed the following features:

- Stellar densities (see scale on right axis) indicates a high concentration of young stars located in the selected regions in relation with the field values, confirming the criteria used in their choice.
- Regarding the color excesses, the three regions are suffering some differential reddening, however it was possible to distinguish a concentration of values on each one. In particular, *R1* and *R2*

this concentration is around $E_{B-V} = 0.33$ and in *R3* it is around $E_{B-V} = 0.43$. On the other hand field stars reveals a wide spread of values with one O-type star with a strong reddening ($E_{B-V} \sim 1$).

- Distance distributions reveal a clear peak in *R1* and *R2* at $V_0 - M_V = 11.8$ and this value could be adopted also as a representative value for a possible stellar group ("a") placed in these regions. In *R3* appears $V_0 - M_V = 12.5$ as a better representative value for another possible stellar group ("b"). Additionally, there is one B-type star at about $V_0 - M_V = 9.25$ located in *R1*, and there are two O-type star at about $V_0 - M_V = 14$, one of them in *R1* and the other in the field. These later two stars could be part of another group of young stars ("c"). There is also a set of B stars covering an important range in distance, from a few hundred pc to at least 1.5-2 kpc with an average stellar density $\sim 60\%$ higher than the average in the solar neighborhood (Allen 1973).

All these facts are reflected in the Two Color (TCDs) and Color Magnitude Diagrams (CMDs) shown in Figs. 3 and 4, respectively. In particular, Fig. 3a reveals the already indicated differential reddening with excess values ranging from 0.28 to 0.45, and Figs. 3b and 3c indicate no evident deviations from the normal reddening law ($R = A_V/E_{B-V} = 3.1$) in the zone, in agreement with previous polarimetric studies (see Vega et al. 1994).

3.2.2 Lower main sequence

To study the lower main sequence (MS) ($V > 14$) we first attempt to quantify field star contamination. To this purpose, we developed a code that performed a statistical decontamination of the field stars over the CMDs (see Gallart et al. 2003). Briefly, the procedure consists in a star-by-star position comparison onto the CMDs of each region (*R1*, *R2* and *R3*) and a CMD of a representative field located near them and covering the same sky area. Then, we subtract field stars with similar position (color and magnitude) from the CMDs to obtain a decontaminated diagram. For this task we used our V vs. $V - I$ diagrams since they are the deepest ones. In Fig. 5 we present the resulting CMDs, where we could identify a highly probable PMS population (small red circles). To strengthen our results, we

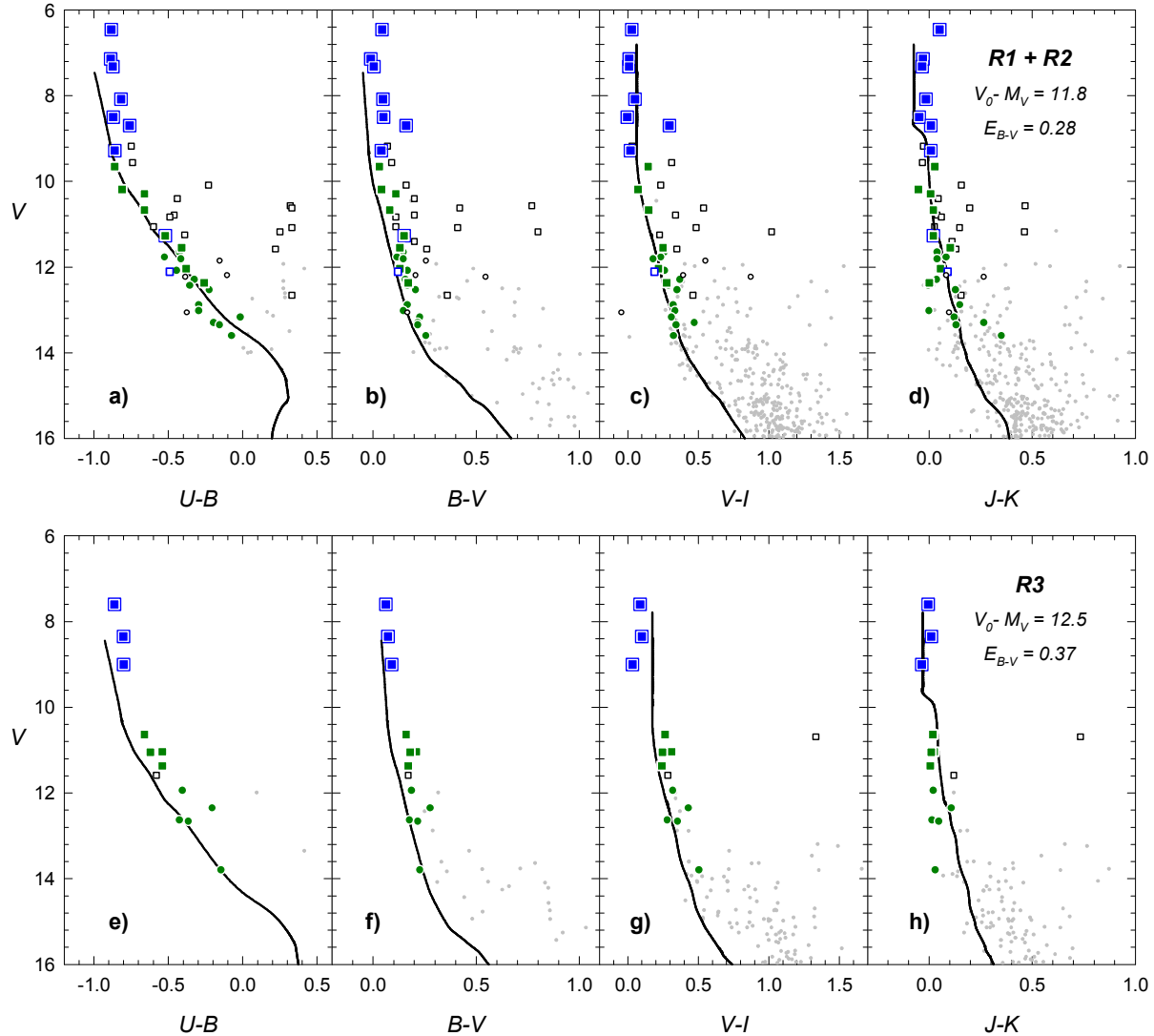


Figure 4. CMDs of stars placed in the three selected regions of the studied zone (see Fig. 1b). Symbols have the same meaning as in that figure. Solid (black) curves are the Schmidt-Kaler (1982) ZAMS (for UBV), the Cousins (1978a,b) MS (for VI) and the Koornneef (1983) MS (for JHK) corrected by the respective adopted color excesses and apparent distance moduli for each stellar group located in each region (see Table 4).

use X-ray data as an additional membership criteria. PMS stars are routinely identified using X-ray emission and this kind of observations should reveal almost all ($\sim 90\%$) the PMS population up to the corresponding detection limit (Feigelson & Getman 2005). Different panels in Fig. 5 (x symbols) reveal their spatial distribution over the three selected regions. We also cross-correlated our data with IR sources present inside these three regions (big grey circles in Fig. 5). In particular, we mark those ones (red triangles) with infrared behavior expected for a young stellar objects (YSOs), say with an infrared rising energy distribution – $F_{21}/F_{14} > 1$ and $F_{14}/F_8 > 1$, (Lumsden et al. 2002).

We could remark the following: a) Most optical sources that could be associated with an X-ray counterpart follow closely the color and magnitude distribution of the stars we selected as probable PMS objects after the field star decontamination. b) The observed width in both set of data could be caused by an age spread, binary stars, accretion stellar discs – Preibisch & Zinnecker (1999); Kenyon & Hartmann (1990) – or/and differential reddening. c) The

amount of X-ray sources is significantly lower than those revealed in the decontamination process; and d) We found only a few probable YSOs (Fig. 5c).

3.3 Stellar groups and selected stars

The analysis in Sect. 3.2.1 allowed us to better understand this particular galactic direction. Previous work by other authors (see Sect. 1) claimed the presence of a spread of early stars along the line of sight or the presence of several stellar groups. Our analysis indicated that we could recognize a spread of early (B-type) star, two main stellar groups and a young background stellar population. Each group exhibit an important dispersion in distance/excesses, that one can explain with spectroscopic errors, and other well known effects such as multiplicity, evolution, fast rotation and/or differential reddening. The main stellar groups/populations can be described as follows:

- "a": This stellar group is located at about 2.3 kpc from the Sun,

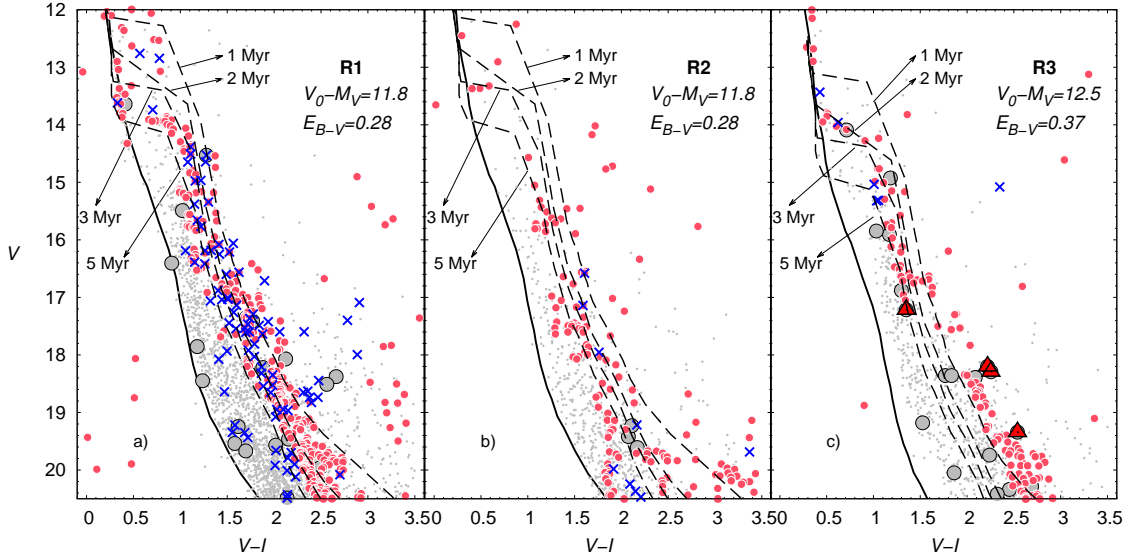


Figure 5. Detailed CMDs of stars located in the three selected regions (grey dots). Solid curves are the Schmidt-Kaler (1982) and Cousins (1978a,b) empirical MS; dashed curves are Siess et al. (2000) isochrones for $z = 0.02$. All the reference curves are corrected by the adopted color excesses values and apparent distance moduli (see Table 4). Red circles are stars resulting from statistical subtraction between each selected region and a comparison region. Blue 'X' are optical sources correlated with X ray sources. Big circles are optical sources correlated with MSX ray ones and red triangles are considered YSOs.

Table 4. Parameters of main stellar groups

Parameter	"a"	"b"	"c"
$V_0 - M_V$	11.8 ± 0.2	12.5 ± 0.2	~ 14
E_{B-V}	0.28-0.40	0.37-0.45	$\sim 1 ?$
<i>Nuclear Age</i> [Myr]	~ 3	~ 3	$\sim 10 ?$
<i>Contraction Age</i> [Myr]	$\sim 3 - 5$	$\sim 2 - 3$	-
<i>IMF slope</i> (Γ) (case a)	-1.00 ± 0.35	-1.02 ± 0.37	-
(case b)	-0.94 ± 0.27	-	-
<i>Total mass</i> [M_\odot] (case a)	$\sim 1100 \pm 200$	$\sim 470 \pm 100$	-
(case b)	$\sim 1200 \pm 200$	-	-
Kinematic values from O member stars			
$\mu_\alpha \cos(\delta)$ [mas/yr]	-5.1 ± 1.2 (7)	-6.1 ± 1.1 (2)*	$\sim -0.2 ?$ (2)
μ_δ [mas/yr]	$+0.2 \pm 1.2$ (7)	-0.7 ± 0.8 (2)*	$\sim -5.6 ?$ (2)
RV_{LSR} [km/s]	$+5.9 \pm 2.8$ (5)**	$+4.4 \pm 0.5$ (2)	$\sim -10.7 ?$ (1)

Notes:

- Number of stars is indicated in parenthesis
- * Star HD 101436 excluded
- ** Stars HD 101205 and HD 101223 excluded
- IMF case a: HD 101205 star was not considered as member
- IMF case b: HD 101205 star was considered as member
- ?: very uncertain values

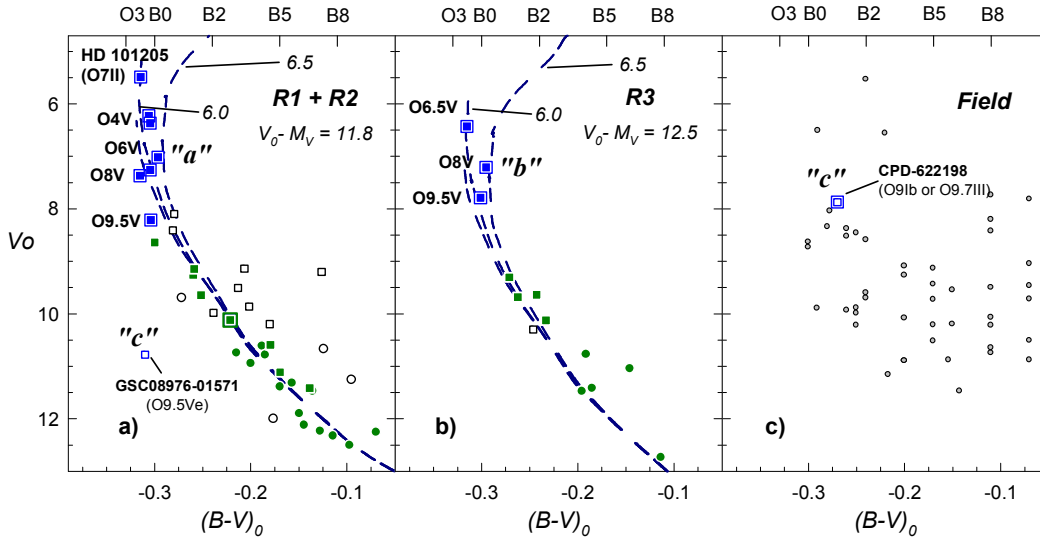


Figure 6. Corrected CMDs of stars presented in Fig. 4. Symbols are as in Fig. 1b. Dashed (blue) curves are Marigo et al. (2008) isochrones for $z = 0.02$ (numbers indicates $\log(\text{age}[\text{yr}])$). All the reference curves are corrected by the respective adopted distance modulus (see Table 4). Upper axis indicate ST for MS stars. O stars representative of each stellar group/population are indicated with letters "a", "b" and "c".

suffering an E_{B-V} ranging from 0.28 to 0.40, and mainly located in R1. However, the brightest stars of R2 revealed similar properties and they were also considered part of the same stellar group.

- "b": This stellar group is at about 3.2 kpc from the Sun, suffering an E_{B-V} ranging from 0.37 to 0.45, and mainly located in R3.

- "c": This is an apparent spread of young background population at about 8 kpc from the Sun, represented in our data by at least two O-type stars.

Under these assumptions and adopting a normal reddening law, we simultaneously fit a zero main sequence (ZAMS) or a MS in all the CMDs (see Fig. 4) at respective main groups distances revealed in Fig. 2. These relationship closely follow both the brightest stars and the fainter B-type ones.

In Fig. 6 we reddening-present the corrected CMDs for brightest ($V < 14$) stars located in R1 + R2, R3 and the field around them in different panels. We use only stars with available spectral classification, or for which it was possible to apply the classic de-reddening method (see Baume et al. 2003) and the relation $E_{U-B}/E_{B-V} = 0.72 + 0.05 E_{B-V}$ (see Fig. ??a). We noticed that in Fig. 6 stars located in R1 + R2 and R3 show consistent magnitude and spectral classification sequences and it seems conceivable to associate most OB stars in each panel with the stellar groups "a" and "b" mentioned above.

A few stars deserve additional comments (see also Fig.6):

- HD 101205: It is the brightest star in the selected regions and is classified at *SIMBAD* as a O8 V but as a O7 II by Sota et al. (2013). In both cases this star do not follow the above indicated sequence and under the former classification it yields an spectroscopic $V_0 - M_V = 10.2$. However, adopting the later classification and considering it is a quadruple system with at least 3 OB components (Sana et al. 2011) it is possible to explain its particular location on Fig.6 and could be considered as a group "a" member.

- CPD-62°2198: This star is placed among other well located MS O-type stars but it is located in the field, outside the selected regions R1, R2 and R3. This star is classified as a supergiant (O9 Ib; *WEBDA*) or as a giant (O9.7 III; Sana et al. 2011) revealing it

could have a spectroscopic distance moduli of 14.2 or 13.0, respectively. In any case this star would be behind the main stellar groups and it would be part of the called population "c".

- HD 101333: This star is also located along a MS (see Fig.6), however it is classified as a giant (O9.5 III; *SIMBAD*) or a dwarf (O9.5 V; Sana et al. 2011). In the former classification it would share the place with CPD-62°2198, but, if a giant, it could still be considered part of the "b" group.

- HD 308804: This star has also different spectral classifications. It is a O9.5 Vn in *SIMBAD* and a B3 V by Sana et al. (2011). As an O-type star, it would have a similar distance as CPD-62°2198. However, by adopting the later spectral type, it could be considered member of the "a" group.

- GSC08976-01571: This star is classified as a O9.5 Ve (*WEBDA*). It is placed in R1 but it is a too faint MS star to belong to the main stellar groups. With a spectroscopic distance $V_0 - M_V = 14.8$ it be a member of the "c" group.

The resulting parameters of the main stellar groups and background stellar population are summarized in Table 4.

3.4 The Galactic spiral structure

Previous investigations –Carraro & Costa (2009), Baume et al. (2009, 2011) and references therein– presented their analysis of optical observations along directions close of the field studied in this paper. In all cases, several early-type star groups (usually three) were detected along the line of sight, and they were considered as belonging to spiral features located at increasing distance from the Sun.

In this work we found several populations of young stars as well, thus lending further support to our earlier results. In this study we found: a) a population represented by several B-type stars scattered form a few hundred of parsecs to at least 1.5-2 kpc of the Sun; b) a second population identified by the young stellar groups "a" and "b" with several O stars situated at 2.3 and 3.2 kpc respectively; and c) a third population which is represented by at least two

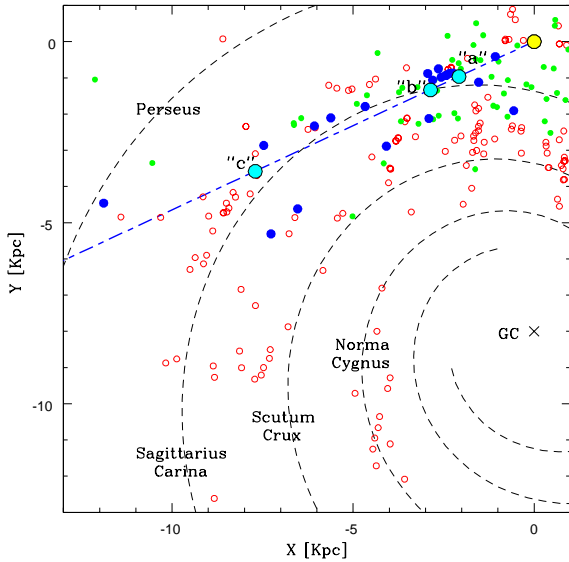


Figure 7. Comparison of the studied Galactic direction (dashed blue line) to the Vallée (2008) model with four arms. The big cyan open circles indicate the studied "a" and "b" stellar groups and the background young stellar population "c" (see Sect. 3.3). We assumed a distance to the Galactic Centre of $R_0 = 8.0$ kpc. Other stellar populations are plotted for reference: (green) points are Cepheid (Majaess et al. 2009); filled (blue) circles are open clusters and young groups from optical ($UBVI$) data (from several studies); and open small (red) circles mark the HII tracers (Hou et al. 2009). The yellow circle marks the position of the Sun.

O stars (one in R1 and other in the field) identified as population "c" and located at about 8 kpc.

The results of this paper together with previous results are presented in Fig. 7 where the Vallée (2008) spiral arms' model is also shown as dotted curves. It reveals then a consistent picture between the described groups/populations and those already known. It seems necessary to study more directions close to this regions using optical and infrared observations of young objects to complete the picture of spiral structure in the fourth Galactic quadrant.

3.5 Dating the stellar groups

In order to estimate the ages of the main stellar groups, we compared our data with different theoretical sets of isochrones over the CMDs and we also took into account the spectral stellar classifications (when available). We considered then two cases:

- For brightest (earlier) stars, we compared their CMD position (see Fig. 6) with models computed for solar metallicity, mass loss and overshooting (Marigo et al. 2008) shifted by adopted distance values for groups "a" ($V_0 - M_V = 11.8$) and "b" ($V_0 - M_V = 12.5$). Intrinsic scatter is present in our data and this fact prevents a unique isochrone solution, however it is still possible to obtain an estimate of the age value for stellar groups "a" and "b", say ~ 3 Myr. This value is consistent with the expected lifetime on the MS of the earlier stars of each group ($\sim O5$). These values obtained for post MS evolution were identified as "nuclear ages". For population "c", we adopted the lifetime of a O9-B0 on MS (~ 10 Myr) as age estimate.

- For the faintest (PMS population) stars, we superimposed a set of Siess et al. (2000) PMS models on CMDs presented in Fig. 5 using the respective E_{B-V} and $V_0 - M_V$ values. The transition from

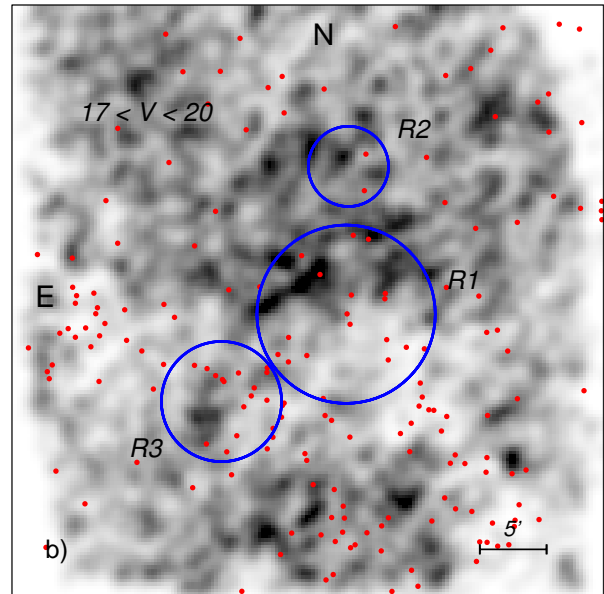
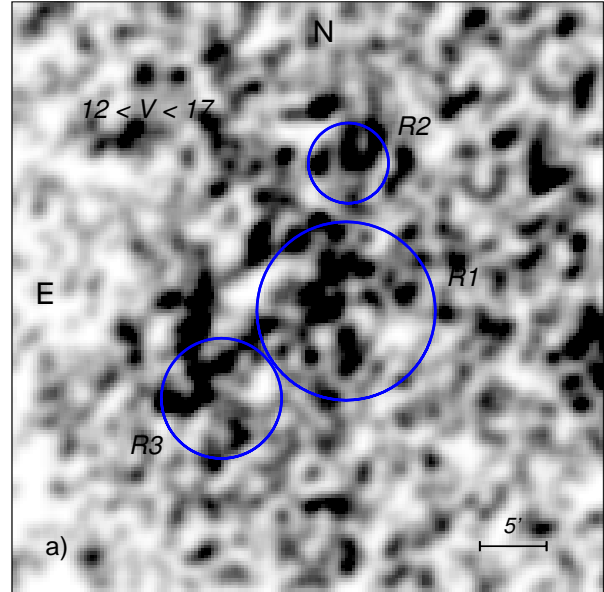


Figure 8. Density maps for stars located between two PMS isochrones (see text). Both panel discriminate stars brighter and fainter than $V = 17$. Blue circles indicate the selected regions. Red dots are MSX sources (Lumsden et al. 2002) correlated with our optical data.

PMS to MS phase is also an extremely accurate age diagnostic. This phase is clearly seen in R1 and in R3, and to less extent in R2 and indicates an age between 2 and 3 Myr. The adopted age values for each group are indicated in Table 4 identified as "contraction ages".

Taking into account the uncertainties in the determinations of the ages and distances, it is possible to conclude that there is no significant difference between the more massive and less massive stars' ages.

3.6 PMS population

Regarding the PMS population, we noticed that most of X-ray sources are distributed uniformly inside *R1* but tend to show uneven distributions between *R1* and the regions *R2* and *R3*, suggesting separated groups. On the other hand, identified YSOs are all placed in *R3* (see Figs. 1b and 5). This difference could be in part real and indicate a different evolutionary stage, but it is more conservatively caused by a distance objects population placed in this region as was suggested by the presence of a recently discovered embedded clusters using data from the deep near infrared VVV⁹ survey (Borissova et al. 2011).

In order to better understand the PMS population distribution in the region, we build the spatial density stellar maps selecting stars placed between the following limits: a PMS isochrone of 1 Myr (at $E_{B-V} = 0.28$ and $V_0 - M_V = 11.8$) and a PMS isochrone of 5 Myr (at $E_{B-V} = 0.37$ and $V_0 - M_V = 12.5$). In this process, we used first the triangles method (Kippenhahn et al. 1967) for the selection over the CMDs of all the observed stars, and then we choose a spatial bin size of 1:0 and the drizzle method (Fruchter & Hook 2002) with a 15'0 step for the building of the density maps. Our results are presented in Fig. 8 where we distinguish stars brighter and fainter than $V = 17$ ($\sim 1.6-2 M_\odot$). We noticed that $V < 17$ stars (Fig. 8a) present over-densities well correlated with the previous selected regions according the MS stars ($V < 12$). On the other hand, $V > 17$ stars (Fig. 8b) only presented an appreciable over-density in the north part of *R1*. We also observed a close correlation between lower density regions in this plot and MSX sources – mainly located at south and east of *R1-R3*. This correlation indicates that this map mainly reflects the differential absorption present across our FOV and not real stellar concentrations.

All these facts reinforce the idea that the PMS population in the studied field is nearly 2 Myr, mainly concentrated in *R1* and could be revealed in our analysis up to $V = 17$. Fainter (less massive) possible PMS population could not be separated from the field population using this method.

3.7 The initial mass function of the main stellar group

The Initial Mass Function (IMF) can be approximated by a power law of form:

$$\log(N/\Delta(\log m)) = \Gamma \log m,$$

where N is the number of star per logarithmic mass bin $\Delta(\log m)$.

We computed the IMFs for groups "a" and "b", using respectively stars located in regions *R1* + *R2* and *R3* (see Sect. 3.3). To build the IMFs, we divided, on each region, the stars in two sets: brighter and fainter than $V = 12$. In the former case, we considered only stars adopted as members following our spectrophotometric analysis (see Sect. 3.2) and individual masses were estimated via a linear interpolation the Marigo et al. (2008) model for 3 Myr. For the latter case, we considered the stars resulting from the statistical decontamination (see Sect. 3.2.2) and we used the Siess et al. (2000) stellar model for 3 Myr for deriving individual masses. We also considered the CFs (see Sect. 2.3) which, however, are important only at very low mass values ($M < 0.5 M_\odot$). Figure 9 shows the resulting IMFs (histograms) and the least square fits to the data (lines). In all these fits we took into account only stars with masses

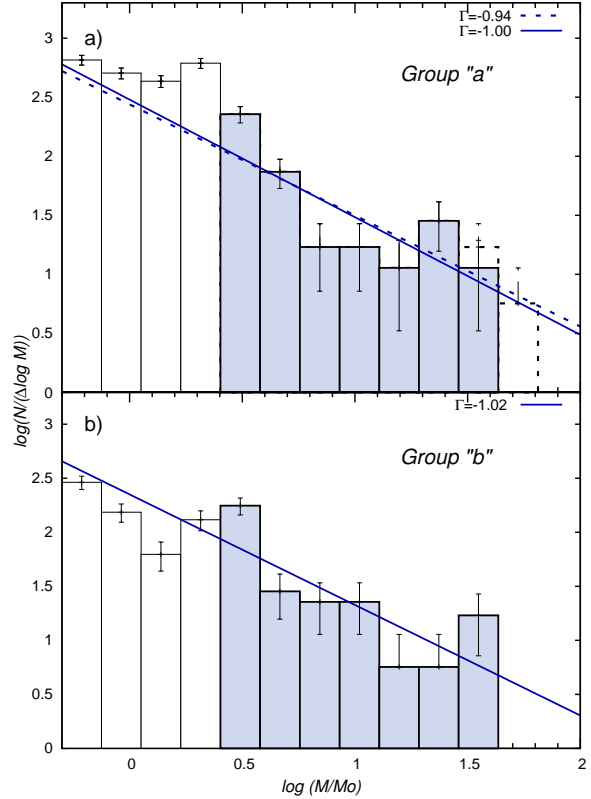


Figure 9. IMFs obtained for the stellar groups "a" and "b" (see Sect. 3.3). For group "a", both cases represent results were HD 101205 was and was not included. Grey bins ($M > 2 M_\odot$) represent values considered to compute the power law fits. Error bars indicate Poisson uncertainty.

larger than $2 M_\odot$. The IMF slopes are reported in Fig. 9 and Table 4. These values nicely compares (within the errors) with the Salpeter (1955) slope ($\Gamma = -1.35$), although they tend to be lower than this value.

We estimated the total mass of the stellar groups integrating over the mass range as follows: individual masses for all the stars with masses greater than $2 M_\odot$ were summed up, while for lower masses we estimated the amount of star at each mass bin using the values given by the power law. The estimated total masses for each stellar group are presented in Table 4.

We repeated the analysis, but using for the faint group only stars with a XMM counterpart. In this case we obtained for each bin smaller numbers of sources ($\sim 15\% - 30\%$), as was expected from a simple visual inspection of Fig. 5. This difference might derive from X-ray data incompleteness and crowding, as previously suggested by Nazé et al. (2013). A similar situation was reported by Prisinzano et al. (2005) in their study of NGC 6530.

3.8 Kinematic study

We extracted heliocentric radial velocities from the WEBDA database for 25 stars (see Sect. 2.4). Since they come from different sources, taken at different epochs and with different spectral dispersions, we averaged the values obtained from better spectral resolution observations. For binary systems, their barycentric radial velocities were computed analysing the best-fitting curves from Gies et al. (2002) and Sana et al. (2011).

⁹ Vista Variables in the Via Lactea

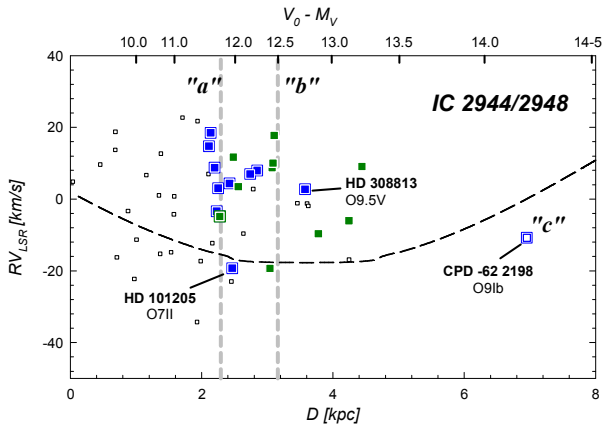


Figure 10. AL fit of the galactic rotation model (dashed curve) applied to our Galaxy (Fich et al. 1989) and LSR radial velocities of stars placed in the studied zone (see Fig. 1). Symbols are the same meaning as in Fig. 1b. Vertical lines indicates the adopted 2.3 and 3.2 kpc distances ($V_0 - M_V = 11.8$ and $V_0 - M_V = 12.5$) for the stellar groups "a" and "b" (see Sect. 3.3)

In order to compare the stellar radial velocities with a model of Galactic rotation, we corrected the heliocentric values to the Local Standard of Rest (LSR). We adopted 13.3 km/s for the solar motion relative to the LSR – $(U, V, W)_\odot = (9.96, 5.25, 7.07)$ km/s – according to Aumer & Binney (2009) and we used the stellar spectrophotometric distances computed in Sect. 3.2.

As for the Galactic rotation curve, we considered the Adjusted Linear Model (AL) and the Power Law Model (Fich et al. 1989). Since, in our case, both models provide similar results, we eventually chose the former. Results are presented in Fig. 10. We computed then the mean LSR velocities of the groups "a" and "b" considering only their O stars. In the case of the population "c", only CPD-62°2198 star provided radial velocity data and it was adopted as a poor representative value for these stars (see Table 4). We then could conclude that stellar groups "a" and "b" (at about 2.3 and 3.2 kpc respectively) do not follow the Galactic rotation model and it is possible that population "c" could have a closer behavior. We noticed that the particular kinematic behavior in radial velocities of the studied stellar groups "a" and "b" could may have been mistakenly interpret an individual member as a run away star. In fact, it could be the case of star HD 101131, since this one was identified as a run away object by van Buren et al. (1995). However, recently this star was only identified as an object with an associated extended source (Peri et al. 2012) with an excess 60μ emission that could be produced by a bow-shock (Noriega-Crespo et al. 1997).

The cross-correlation of our photometric data against the UCAC4 catalog allows us to analyze also the proper motion of more than 7500 stars in the studied area (see Fig. 1). Figure 11 presents the Vector Point Diagram (VPD), where we marked previously identified stars (as in Fig. 1b). Most of O stars considered stellar groups "a" or "b" members show quite a similar motion. On the other hand, O stars identifying population "c" (hollow blue symbols) seems to show again a different kinematic behavior. We adopted then the averaged proper motions of O stars of each group as representative of each one and are presented in Table 4.

The kinematic information for brightest stars in the studied region was summarized in Table 5.

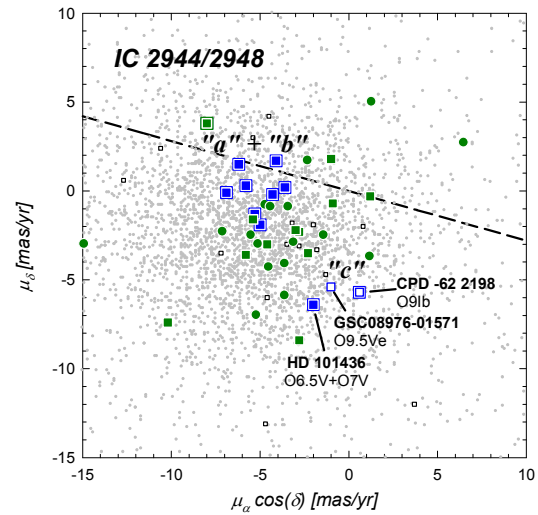


Figure 11. VPD for the stars brighter than $V = 16$. Symbols are the same meaning as in Fig. 1b. Dashed line indicates expected direction for movements parallel to the Galactic plane.

4 CONCLUSIONS

In this study we reported on a deep optical photometric study of the region surrounding IC 2944/2948 at $(l \sim 294.8; b \sim -1.6)$. Optical photometry was complemented with archival data, which include astrometry, shallow optical, IR and mid-IR photometry, and spectroscopy. This region harbors a wealth of young stars, emission nebulae, compact dark clouds and probable YSOs. Out of this material, we could derive the main properties of different populations located in the area.

First, we could assess that there are several populations along this particular line of sight: we could describe an spreading population of B-type stars with an important range in distance, two stellar concentrations ("a" and "b") located at ~ 2.3 and ~ 3.2 kpc, and some early stars ("c") apparently representing a young population located as distant as 8 kpc.

Second, by focusing our attention on the main stellar concentrations, we revealed that they are hosting a relevant population of PMS stars and are as young as 2-3 Myrs. We derived their IMFs and we found their slope for massive stars is low but still compatible with the standard Salpeter law, and we also provided an estimate of each stellar group in ~ 1100 and $\sim 500 M_\odot$.

Third, we found that all O stars in these two groups share similar kinematics and their representative values are different from that expected from Galactic rotation models in this part of the Milky Way. Regarding the mentioned young background population ("c"), we found it could had an apparent different kinematics we estimated an age of ~ 10 Myr as a crude approximation.

Finally, we compared all these populations locations and characteristic with those results obtained at similar directions of the Galaxy and their are consistent with the idea of an almost tangent view along of the Sagittarius-Carina spiral arm. In particular, groups "a" and "b" would coincide with the near side of this arm, while group "c" with the far side, and the spread of B stars a continuous young population characteristic of a grand design spiral structure.

Table 5. Kinematic information for studied OB stars

Name	RV_{LSR} [km s ⁻¹]	N ^(*)	$\mu_{\alpha} \cos \delta$ [mas yr ⁻¹]	μ_{δ} [mas yr ⁻¹]	Binarity	RV Source
HD101205	-19 (20)		-6.2 (1.0)	1.5 (1.0)	SB2 ^b	Kharchenko (2007)
HD101131	9 (11)	75	-5.8 (1.0)	0.3 (1.0)	SB2 ^a	Gies et al. (2002)
HD101190	8 (9)	20	-4.1 (1.0)	1.7 (1.0)	SB2 ^b	Sana et al. (2011)
HD101436	4 (10)	13	-2.0 (1.6)	-6.4 (4.2)	SB2 ^b	Sana et al. (2011)
HD101298	7 (8)	3	-3.6 (1.2)	0.2 (1.2)	SB? ^b	Trackeray & Wesselink (1965)
HD101413	18 (16)	14	-6.9 (1.3)	-0.1 (1.4)	SB2 ^b	Conti et al. (1977)
HD101191	3 (7)	3	-6.9 (1.2)	-0.1 (1.2)	SB ^b	Trackeray & Wesselink (1965)
HD101223	15 (7)	3	-5.0 (1.3)	-1.9 (1.7)	SB? ^b	Trackeray & Wesselink (1965)
HD101333	-3 (5)	3	-5.3 (1.3)	-1.3 (1.3)	SB? ^b	Huang & Gies (2006)
HD308813	3 (22)	3	-4.3 (1.4)	-0.2 (1.3)	SB ^b	Huang & Gies (2006)
HD308818	9 (7)		-2.8 (5.1)	-2.3 (1.3)		Karchenko (2007)
CPD-62°2153	18 (7)		-2.3 (1.1)	-3.5 (1.3)		Karchenko (2007)
HD308826	12 (-)		-3.0 (2.3)	-2.2 (2.0)		SIMBAD
HD308825	-6 (0)	3	-4.6 (1.3)	-3.0 (3.1)		Huang & Gies (2006)
HD308817	10 (9)	3	-10.2 (1.4)	-7.4 (1.6)		Huang & Gies (2006)
CPD-62°2198	-11 (4)	3	0.6 (1.1)	-5.7 (1.0)	SB? ^b	Huang & Gies (2006)
HD308831	-19 (10)	3	-1.0 (3.1)	1.8 (3.5)		Huang & Gies (2006)
HD308833	-10 (9)	3	1.2 (1.7)	-0.3 (2.4)		Huang & Gies (2006)
HD308804	-5 (3)	3	-8.0 (1.5)	3.8 (2.6)	SB? ^b	Huang & Gies (2006)
HD308832	9 (2)	3	-5.8 (1.8)	-3.6 (1.7)		Huang & Gies (2006)
GSC08976-00983	3 (7)	3	-0.9 (1.9)	-0.7 (1.7)		Huang & Gies (2006)

Notes:

- (*) = Number of averaged spectra
- Errors are presented in brackets
- Binarity source: *a* = Gies et al. (2002); *b* = Sana et al. (2011)
- SB = Binary system, single spectra; SB2 = Binary system, double spectra; SB? = Dubious binary system (possible binary systems by Ardeberg & Maurice (1977) but probable single star by Sana et al. (2011))

ACKNOWLEDGMENTS

GB, MJR, MAC and JAP acknowledges support from CONICET (PIPs 112-201101-00301 and 112-201201-00226). The authors are much obliged for the use of the NASA Astrophysics Data System, of the *SIMBAD* database and *ALADIN* tools (Centre de Données Stellaires — Strasbourg, France), and of the WEBDA open cluster database. This publication also made use of data from: a) the Two Micron All Sky Survey, which is a joint project of the University of Massachusetts and the Infrared Processing and Analysis Center/California Institute of Technology, funded by the National Aeronautics and Space Administration and the National Science Foundation; b) the AAVSO Photometric All-Sky Survey (APASS), funded by the Robert Martin Ayers Sciences Fund. c) the Midcourse Space Experiment (MSX). Processing of the data was funded by the Ballistic Missile Defense Organization with additional support from NASA Office of Space Science. We thank R. Martínez and H. Viturro for technical support. Finally, we thank the referee, whose comments helped to improve significantly the paper.

REFERENCES

- Alter, G., Balazs, B., & Ruprecht, J., eds. 1970, Catalogue of Star Clusters and Associations (2d ed. ; Budapest: Akad. Kiado)
- Allen, C. W. 1973. *Astrophysical Quantities*, Third Edition. University of London, The Athlone Press.
- Anderson, E., & Francis, C. 2012, *Astronomy Letters*, 38, 331
- Ardeberg, A., & Maurice, E. 1977, *A&AS*, 28, 153
- Ardeberg, A., & Maurice, E. 1980, *A&AS*, 39, 325
- Ardeberg, A., & Maurice, E. 1981, *A&A*, 98, 9
- Aumer, M., & Binney, J. J. 2009, *MNRAS*, 397, 1286
- Baume, G., Vázquez, R. A., Carraro, G., & Feinstein, A. 2003, *A&A*, 402, 549
- Baume, G., Carraro, G., & Momany, Y. 2009, *MNRAS*, 398, 221
- Baume, G., Carraro, G., Comeron, F., & de Elía, G. C. 2011, *A&A*, 531, A73
- Borissova, J., Bonatto, C., Kurtev, R., et al. 2011, *A&A*, 532, A131
- Carraro, G., 2013, *Proceedings of the IAU Symposium No. 298*, "Setting the scene for Gaia and LAMOST", eds. S. Feltzing, G. Zhao, N. A. Walton, and P. A. Whitelock, in press (arXiv:1307.0569)
- Carraro, G., & Costa, E. 2009, *A&A*, 493, 71
- Corti, M. A., Arnal, E. M., & Orellana, R. B. 2012, *A&A*, 546, A62
- Corti, M. A., & Orellana, R. B. 2013, *A&A*, 553, A108
- Conti, P. S., Leep, E. M., & Lorre, J. J. 1977, *ApJ*, 214, 759
- Cousins, A. W. J. 1978, *Monthly Notes of the Astronomical Society of South Africa*, 37, 62
- Cousins, A. W. J. 1978, *Monthly Notes of the Astronomical Society of South Africa*, 37, 77 errata
- Egan, M. P., Price, S. D., Kraemer, K. E., et al. 2003, *VizieR Online Data Catalog*, 5114, 0
- Fich, M., Blitz, L., & Stark, A. A. 1989, *ApJ*, 342, 272

- Feigelson, E. D., & Getman, K. V. 2005, arXiv:astro-ph/0501207
- Fruchter, A. S., & Hook, R. N. 2002, PASP, 114, 144
- Gallart, C., Zoccali, M., Bertelli, G., et al. 2003, AJ, 125, 742
- Gies, D. R., Penny, L. R., Mayer, P., Drechsel, H., & Lorenz, R. 2002, ApJ, 574, 957
- Henden, A. A., Terrell, D., Welch, D., & Smith, T. C. 2010, Bulletin of the American Astronomical Society, 42, 515
- Hou, L. G., Han, J. L., & Shi, W. B. 2009, A&A, 499, 473
- Huang, W., & Gies, D. R. 2006, ApJ, 648, 580
- Jester, S., Schneider, D. P., Richards, G. T., et al. 2005, AJ, 130, 873
- Kenyon, S. J., & Hartmann, L. W. 1990, ApJ, 349, 197
- Kharchenko, N. V., Scholz, R.-D., Piskunov, A. E., Röser, S., & Schilbach, E. 2007, Astronomische Nachrichten, 328, 889
- Kharchenko, N. V., & Roeser, S. 2009, VizieR Online Data Catalog, 1280, 0
- Kippenhahn, R., Weigert, A., Hofmeister, E., 1967, "Methods for Computational Physics", Vol. 7 in Alder B., P.129 New York Academic Press
- Koornneef, J. 1983, A&A, 128, 84
- Lada, C. J. & Lada, E. A., 2003, ARA&A, 41, 57
- Lumsden, S. L., Hoare, M. G., Oudmaijer, R. D., & Richards, D. 2002, MNRAS, 336, 621
- Majaess, D. J., Turner, D. G., & Lane, D. J. 2009, MNRAS, 398, 263
- Marigo, P., Girardi, L., Bressan, A., et al. 2008, A&A, 482, 883
- Martins, F., & Plez, B. 2006, A&A, 457, 637
- McSwain, M. V., & Gies, D. R. 2005, ApJS, 161, 118
- Nazé, Y., Rauw, G., Sana, H., & Corcoran, M. F. 2013, A&A, 555, A83
- Noriega-Crespo, A., van Buren, D., & Dgani, R. 1997, AJ, 113, 780
- Peri, C. S., Benaglia, P., Brookes, D. P., Stevens, I. R., & Isequilla, N. L. 2012, A&A, 538, A108
- Perry, C. L., & Landolt, A. U. 1986, AJ, 92, 844
- Preibisch, T., & Zinnecker, H. 1999, AJ, 117, 2381
- Prisinzano, L., Damiani, F., Micela, G., & Sciortino, S. 2005, A&A, 430, 941
- Reipurth, B., Corporon, P., Olberg, M., & Tenorio-Tagle, G. 1997, A&A, 327, 1185
- Reipurth, B. 2008, Handbook of Star Forming Regions, Vol. II
- Salpeter, E. E. 1955, ApJ, 121, 161
- Sana, H., James, G., & Gosset, E. 2011, MNRAS, 416, 817
- Schmidt-Kaler, Th. 1982, Landolt-Börnstein, Numerical data and Functional Relationships in Science and Technology, New Series, Group VI, Vol. 2(b), ed. K. Schaifers, & H. H. Voigt (Berlin: Springer Verlag), 14
- Siess, L., Dufour, E., & Forestini, M. 2000, A&A, 358, 593
- Skrutskie, M. F., Cutri, R. M., Stiening, R., et al. 2006, AJ, 131, 1163
- Sota, A., Maíz Apellániz, J., Morrell, N. I., et al. 2013, arXiv:1312.6222
- Stetson, P. B. 1987, PASP, 99, 191
- Stetson, P. B. 1992, in Stellar Photometry-Current Techniques and Future Developments, ed. C. J. Bulter, & I. Elliot (Cambridge: Cambridge University Press), IAU Coll., 136, 291
- Thackeray, A. D., & Wesselink, A. J. 1965, MNRAS, 131, 121
- Vallée, J. P. 2008, AJ, 135, 1301
- van Buren, D., Noriega-Crespo, A., & Dgani, R. 1995, AJ, 110, 2914
- Vega, E. I., Orsatti, A. M., & Marraco, H. G. 1994, AJ, 108, 1834
- Walborn, N. R. 1972, AJ, 77, 312
- Walborn, N. R. 1987, AJ, 93, 868
- Zacharias, N., Finch, C. T., Girard, T. M., et al. 2013, AJ, 145, 44
- Zwicky, F. 1957, PASP, 69, 518